Improving Diffraction Tomography for Microwave Imaging

N. Baktash
Yazd University
neda_baktash@yahoo.com

Dr. M. Nakhkash
Yazd University
mnakhkash@yahoo.com

Abstract: *Tomography refers to the cross-sectional imaging of an object from either transmission or reflection data collected by illuminating the object from many different directions. The impact of this technique in diagnostic medicine has been revolutionary, since it has enabled doctors to view internal organs with unprecedented precision and safety to the patient. The first medical application utilized x-rays for forming images of tissues based on their x-ray attenuation coefficient. More recently, however, medical imaging has also been successfully accomplished with radioisotopes, ultrasound and magnetic resonance; the imaged parameter being different in each case.*
But, when an object is illuminated with a diffracting source; as is the case with ultrasound and microwaves, the wave field is scattered in practically all directions. In these cases, there is the problem of lack of efficient algorithms to reconstruct a high-quality image. To overcome this problem, one approach is to use diffraction tomography, which is applicable to microwave imaging of biological bodies.
The proposed research aims at describing how to apply the theory to actual problems in medical imaging and other fields. Finally, compare some of reconstruction examples of permittivity and conductivity with our simulation sources.

Keywords: Diffraction tomography, Microwave Imaging, Filtered backpropagation.

1 Introduction

Noninvasive diagnostics using electromagnetic waves are very appealing in several areas of industrial applications, which include civil engineering, nondestructive testing. Geophysical prospecting and biomedical engineering. One particular promising technique is the use of microwave imaging(MI).This technique relies upon the information contained in electromagnetic wave at microwave frequencies to reconstruct some important parameters (such as shapes, locations, etc.) of the objects under test.
The application of Microwave Imaging (MI) to biomedical engineering has many potential advantages over existing techniques. It allows one to obtain the distribution of the complex dielectric permittivity of a tissue, from which biohazard due to undesired exposure can be evaluated. One important area of applications of MI is concerned with the detection of breast cancer. Due to high contrast in the dielectric properties between normal and malignant breast tissues, MI would result in low rate false diagnoses [1]-[3]. In addition, diagnostic systems based on MI could be considerably cheaper and potentially less harmful.
However, the use of MI as a reliable medical diagnostic still needs further development. MI is not at present competitive with other diagnostic techniques, in spite of its definite advantages. The main problem is lack of efficient algorithms, which can derive in real time from microwave data the properties of an object under test in 3 dimensions. The derivation of such information, from physical point of view, is in essence an inverse scattering problem. Recasting as an optimization process, one may solve inverse problems by the use of optimization methods such as gauss-Newton, gradient Iterative and Genetic algorithm methods [4]-[7]. This approach, known as spatial-iterative, gives accurate reconstruction while introduces huge computational burden.

Therefore, spatial-iterative methods cannot be realized in real time and even near-real time with the present computing facilities.

Another approach is to use diffraction tomography (DT), an inversion scheme that reconstructs profile of a weakly scattering object under Born or Rytov approximation. This scheme has been applied to widely scientific discipline including electromagnetic subsurface surveying [8], [9], medical ultrasonic tomography [10] and medical optical tomography [11]. Using FFT for obtaining the image, such an approach is computationally efficient and comparatively straightforward. The success of the DT, however, depends on the validity of the underlying approximations that make the inverse problem linear. It fails to image or provide poor reconstruction for objects having large discontinuities in the permittivity (strong scattering objects) being successful in some extent, alternative versions of the DT [12]-[14] have been proposed to alleviate this drawback.

Our aim of this research was to evaluate the merits of the DT for microwave imaging (especially for breast cancer detection). Direct Fourier (DF) and filtered-backpropagation (FBP) algorithms are implemented within Matlab environment and tested using synthetic data. We generated the data on several cylindrical models by an electromagnetic simulation software. The results and the milestones to reach a practical imaging system will be addressed.

2 Theory and Formulation of the problem

2.1 Diffraction Tomography

Meuller et al [15] initially proposed the configuration shown in Figure 1 for a 2-dimensional DT imaging. A monochromatic (single time frequency) plane wave, having angle φ with x-axis, is incident on an object. The total field is recorded on line TT', outside the object and perpendicular to the propagation direction. The system acquires data for different angles $\varphi_n = 2\pi\pi/N \;\; n = 0,1,\ldots,N-1$ .This scan scenario, originally, inspire from X-ray computerized tomography (CT).

If we assume $E = E^{inc} + E^{sca}$, the scattered field E^{sca} on line TT' is obtained by deducting the total field from the incident plane wave E^{inc}. Generalized projection-slice theorem states: *the Fourier transform of E^{sca} along line TT' gives the values of the 2-D Fourier transform of the object function $O(r)$ along semi-circular arc BOA depicted in Figure 1(b)*. In order to illustrate this theorem, consider the medium is nonmagnetic($\mu = \mu_0$), $\varepsilon = \varepsilon_0 \varepsilon_r$ permittivity, σ conductivity and an incident plane wave traveling in direction $+\eta$ which is formulated as

$$E^{inc}(r) = E_0 \quad exp(jk_0\eta) \tag{1}$$

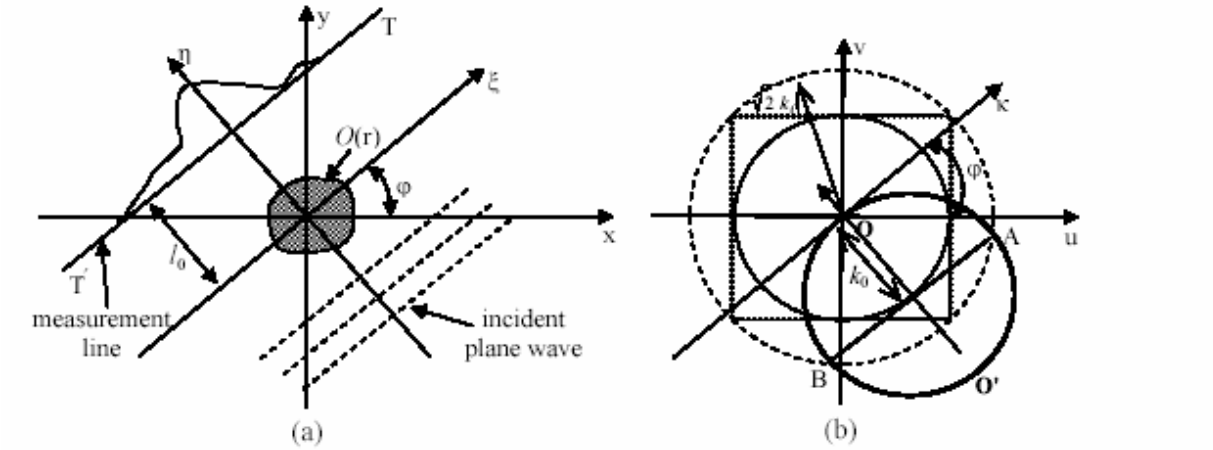

Figure 1: Classical scan configuration of diffraction tomography. a) space domain. b) frequency domain

where (ξ, η) denote the rotated *(x,y)* coordinates(Figure 1). The interaction of the incident wave with the object results in the formation of the wavefield *E(r)* that satisfies the time-independent inhomogeneous Helmholtz equation in born approximation

$$E^{sca}(r) = k_0 \int G(r-r')O(r')E^{inc}(r')d^3r' \tag{2}$$

where $O(r) = \varepsilon_r^c - 1 = \frac{\varepsilon_r}{\varepsilon_{Br}} - 1 + \frac{\sigma}{j\omega\varepsilon_B}$ is the object function and $k_0^2 = \omega^2 \mu_0 \varepsilon_B$ is the wave number.

The 2-D Green function is given by

$$G(r-r') = \frac{j}{4\pi}\int_{-\infty}^{+\infty} exp[j\kappa(\xi-\xi')]\frac{exp\left[j\gamma|\eta-\eta'|\right]}{\gamma}d\kappa \qquad (3)$$

$$, \; r=(\xi,\eta) \; , \; \gamma=\sqrt{k_0^2-\kappa^2}$$

Inserting Equation(1) and Equation(3) into 2-D version of Equation(2), the measured field on line TT' can be obtained by replacing η with l_0

$$E^{sca}(\xi,l_0) = \frac{jE_0k_0^2}{4\pi}\int_{-\infty}^{+\infty}\frac{exp(j\gamma l_0)}{\gamma}exp(j\kappa\xi) \left[\iint_{\Re} O(\xi',\eta')exp[-j\kappa\xi']exp\left[-j(\gamma-k_0)\eta'\right]d\xi'\,d\eta'\right]d\kappa \qquad (4)$$

$\Re$ defines the scattering region, i.e. $\Re = \{(\xi,\eta) \mid O(\xi,\mu)\neq 0\}$.The double integral inside the parentheses in Equation(4) defines 2-D spatial Fourier transform of $O(\xi,\eta)$ at spatial angular frequency of $(\kappa,\gamma-k_0)$. By denoting $\tilde{O}(\kappa,\vartheta)$ as 2-D Fourier transform for $O(\xi,\eta)$, we reach

$$E^{sca}(\xi,l_0) = \frac{jE_0k_0^2}{2}\left\{\frac{1}{2\pi}\int_{-\infty}^{+\infty}\left[\frac{exp\left[j\gamma l_0\right]}{\gamma}\tilde{O}(\kappa,\gamma-k_0)\right]exp(j\kappa\xi)d\kappa\right\} \qquad (5)$$

it could be realize that the term bounded by {} in Equation (5) provides the 1-D inverse Fourier transform of $\tilde{O}(\kappa,\gamma-k_0)exp(j\gamma l_0)/\gamma$ .Therefore Taking Fourier transform of both sides of Equation(5) with regards to variable ξ results in

$$\tilde{O}(\kappa,\gamma-k_0) = \frac{2}{jE_0k_0^2}\gamma \quad exp(-j\gamma l_0)\tilde{E}^{sca}(\kappa,l_0) \qquad (6)$$

Considering $\gamma-k_0=\sqrt{k_0^2-\kappa^2}-k_0$, as κ varies from $-k_0$ to k_0, the coordinates $(\kappa,\gamma-k_0)$ in the frequency domain trace out a semi-circular arc in the *(u, v)*- plane as illustrated in Figure 1(b).

If the scattered field is measured along a line at $\eta=-l_0$, i.e. the reflected field from the object is recorded, a similar procedure derives the following expression which for $\kappa\in[-k_0,k_0]$, the coordinates $(\kappa,-\gamma-k_0)$ are located on semi-circular arc BO'A(Figure 1(b)).

$$\tilde{O}(\kappa,-\gamma-k_0) = \frac{2}{jE_0k_0^2}\gamma \quad exp(-j\gamma l_0)\tilde{E}^{sca}(\kappa,-l_0) \qquad (7)$$

Hence, the Fourier transform of the object function along BO'A can be obtained using the reflected field. In classical DT, the imaging is based on Equation (6), i.e. the transmission field measurements.

It is more instructive to rewrite Equation (6) as

$$\tilde{O}(\kappa,\varphi) = \frac{2}{jE_0k_0^2}\gamma \quad exp(-j\gamma l_0)\tilde{E}^{sca}(\kappa,\varphi) \qquad (8)$$

that clarifies the dependency on the scan angle φ. According to Equation (8), the rotation of the object from $\varphi=0$ to $\varphi=2\pi$ yields the 2-D Fourier transform of *O(x, y)* ($\tilde{O}(u,v)$) on disk with radius $\sqrt{2}k_0$. Due to finite number of the scan angles, the values of $\tilde{O}(u,v)$ can be obtained at some sample points on this disk. In order to reconstruct the object function from these samples, two algorithms have been proposed. The next subsections describe them.

2.2 Direct Fourier

The direct Fourier (DF) method finds the object function from direct 2-D inversion of the frequency domain information. This needs the frequency domain samples are available on a rectangular grid I *(u,v)* plane. However, Equation (8) provides the samples over circular arcs. Thus, the data on the rectangular grid is found with interpolating the samples over the arcs. Scanning the angles from 0 to 2π, the arcs OA and OB in Figure 1(b) span the same disk independently, i.e. there is double coverage of the frequency domain. The frequency samples for arcs (either OA or OB) are, individually, uniform in parameters (κ,φ) , whereas their combination would not present a uniform distribution. As the data should be uniform for interpolation, the samples from one arc (either OA or OB) will be used.

For interpolation, one needs a relationship between *(u,v)* and (κ,φ). As arcs OA and OB covers the same points (double coverage), there would be two separate relationships. Let (κ_1,φ_1) and (κ_2,φ_2) denote the points generated by OA and OB, respectively, and let us convert *(u,v)* to polar coordinates (w,θ) as

$$w=\sqrt{u^2+v^2} \qquad , \qquad \theta = tan^{-1}\left(\frac{v}{u}\right) \qquad (9)$$

With regard to Figure 1(b), (κ_1,φ_1) is given by [16]

$$\kappa_1 = k_0 sin\alpha \quad , \varphi_1 = \theta+\frac{\alpha}{2} \quad , \alpha = 2sin^{-1}\frac{w}{2k_0} \qquad (10)$$

and (κ_2,φ_2) is equal to

$$\kappa_1 = -k_0 \sin\alpha \quad , \varphi_1 = \pi + \theta - \frac{\alpha}{2} \quad , \alpha = 2\sin^{-1}\frac{w}{2k_0} \qquad (11)$$

The algorithm may use different 2-D interpolation techniques, such as nearest neighbour, spline and the interpolation based on circular sampling theorem. The bilinear interpolation, however, has proved to be computationally efficient and give good reconstruction [16]. Based on the DF algorithm, a Matlab program has been prepared which implements the zero-padding technique as well; and allows the user specify the amount of increase in the density. The reconstruction examples will be presented in Section3.

2.3 Filtered-BackPropagation

Devaney [17] has derived filtered-backpropagation (FBP) method, which is similar to the filtered backprojection technique in X-ray tomography. The FBP algorithm has demonstrated to provide the best reconstruction, but it is computationally less efficient than DF technique.

Let obtain the object function from its 2-D frequency components

$$O(x,y) = \frac{1}{4\pi^2}\iint \tilde{O}(u,v)\exp(jxu + jyv)\,dv\,du \qquad (12)$$

In FBP formulation, the above integral is written in terms of (κ,φ) parameters. This is done first by the change of *(u,v)* to polar coordinates with regard to Equations (9) and (10). Also we assume the samples are, only, available on a disk with radius $\sqrt{2}k_0$. Then, replace *(x,y)* with the rotated coordinates (ξ,η) (φ_1 rotation). That is

$$\begin{aligned} &x = \xi\cos\varphi_1 - \eta\sin\varphi_1 \quad , y = \xi\sin\varphi_1 + \eta\cos\varphi_1 \\ &x\cos\theta + y\sin\theta = \xi\cos(\theta - \varphi_1) + \eta\sin(\theta - \varphi_1) \end{aligned} \qquad (13)$$

Substitution the changes in Equation (12) and also to reduce the effect of noise assume both arcs OA and OB have the same angles, i.e. $\varphi_1 = \varphi_2 = \varphi$,and $\kappa_2 = -\kappa_1 = -\kappa$ results in

$$O(x,y) = \frac{1}{j2\pi^2 k_0 E_0}\left\{\int_0^{2\pi}\left[\frac{1}{2\pi}\int_{-k_0}^{k_0} \tilde{H}(\kappa,\varphi,\eta)\exp(j\kappa\xi)\,d\kappa\right]d\varphi\right\} \qquad (14)$$

where

$$\tilde{H}(\kappa,\varphi,\eta) = \tilde{E}(\kappa,\varphi)|\kappa|\exp(-j\gamma l_0)\exp[j(\gamma - k_0)\eta] \qquad (15)$$

The expression inside square parenthesis in Equation(14) defines 1-D inverse Fourier transform of $\tilde{H}$. Denoting H as Fourier inversion of $\tilde{H}$ and considering

$$\xi = x\cos\varphi + y\sin\varphi \quad , \eta = y\cos\varphi - x\sin\varphi \qquad (16)$$

the reconstruction equation can be expressed as

$$O(x,y) = \frac{1}{j2\pi k_0 E_0}\int_0^{2\pi} H(\xi,\eta,\varphi)\,d\varphi \qquad (17)$$

The dependency of $\tilde{H}$ on η reveals that several 1-D Fourier inversion are required so as to attain H for a given (ξ,η) grid, making the FBP algorithm computationally expensive. Nevertheless, the FBP can find *O(x,y)* in any specific region; this could computation burden if the region is small in some applications.

A Matlab program has been written for implementation of the FBP algorithm. The reconstruction examples will be presented in the next subsection.

3 Reconstruction Examples

The following examples are aimed at the evaluation of the DT using both DF and FBP algorithms. By using an electromagnetic simulation software the scattered field data generated on 2-D models. Since, the simulations take a considerable amount of time, the models are chosen to have cylindrical symmetry, which means the models (objects) properties vary only with radial distance from the object centre. For all reconstruction examples, the scan angles are $\phi_n = n2\pi\pi/7, \quad n = 0,1,\ldots,71$ that means $\Delta\varphi_n = 5$ degree. Also, the background medium is presumably free space ($\varepsilon_{Br} = 1$), unless it is specified. Due to the symmetry of circular cylinders, the figures show the profile of either relative permittivity (ε_r) or conductivity along the diameter of the cylinders. Additionally, to discuss the results, we need the definition of two error appear in the reconstructions: 1- the error due to the lack of enough resolution that is referred as to resolution error; 2- the Born error that is because of the Born approximation.

Figure 2 illustrates the first reconstruction using the DF and FBP algorithms. It can be seen that the FBP presents better results at all three frequencies. For both methods, the low-pass filtered version of the object function is obtained, since all spatial frequency components of *O(x,y)* are not available. The figure demonstrates that the increase of the time frequency (*1.0 GHz* to *4.0 GHz*) improves the resolution, which can be justified by noting k_0 becomes larger.

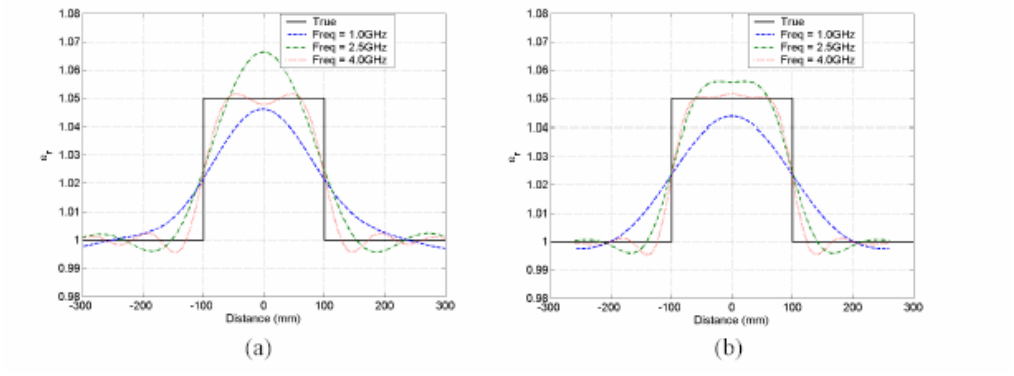

Figure2: Reconstruction of permittivity profile of a cylinder with radius=10cm, ε_r =1.05 and σ =0. a) Using the DF method. b) Using the FBP method.

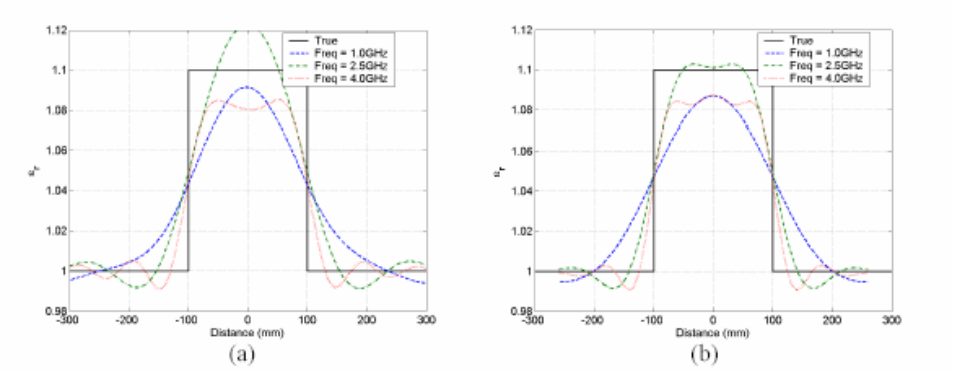

Figure3: Reconstruction of permittivity profile of a cylinder with radius=10cm, ε_r =1.1 and σ =0. a) Using the DF method. b) Using the FBP method.

Figure 3 illustrates how the DF and FBP find the profile of a cylinder with ε_r =1.1. It is evident the reconstruction is not as good s the pervious one, since the higher the permittivity is, the larger the Born error becomes. Also, one can observe that although the growth of the time frequency enhances the resolution, matching between the reconstruction and the true profile is degraded. As the wavelength is decreased (the time frequency is enlarged), the resolution error is reduced; but the Born error contributes more. The FBP algorithm, again, provides the superior results; the reconstruction from the FBP technique are, therefore, only given afterwards.

When the contrast between the object and the background medium is enlarged, the DF fails to image the object, as this fact is pointed out in Figure 4. Furthermore, this failure affects the conductivity profile. Finding the conductivity of the same cylinders (in Figure 4), the FBP provides the result in Figure 5. It can be seen that the error in the conductivity bears higher error when the permittivity contrast is increased, though the object is lossless (i.e. σ =0).

In order to understand the behaviour of the FBP when the object in Figure 3(b) expect with σ =10mS. Figure 6 shows both the permittivity and conductivity.

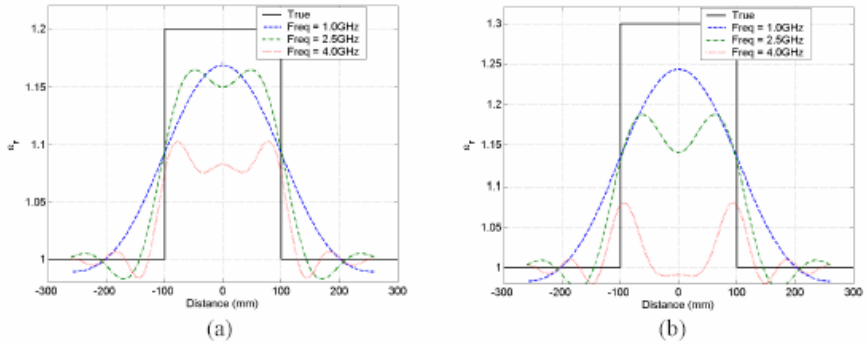

Figure4: Performance of the FBP in obtaining the profile of cylinders with a) ε_r =1.2 and b) ε_r =1.3. In both case, σ =0.

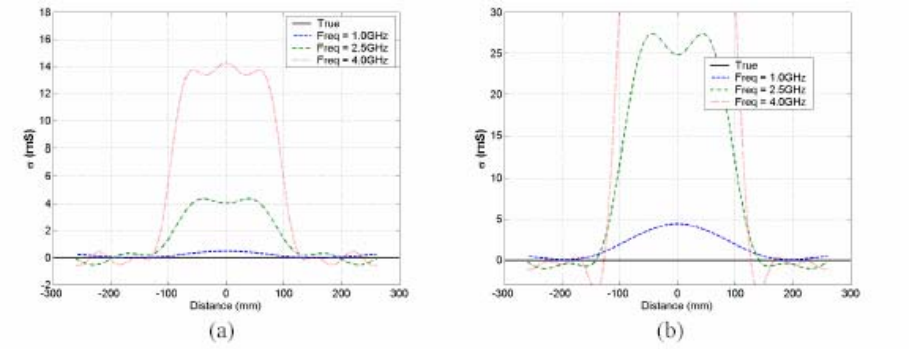

Figure5: Derivation of the conductivity profile by the FBP algorithm. a) the object permittivity is the solid line in Figure 4(a). b)the object has the permittivity profile shown by solid line in Figure 4(b) is the object.

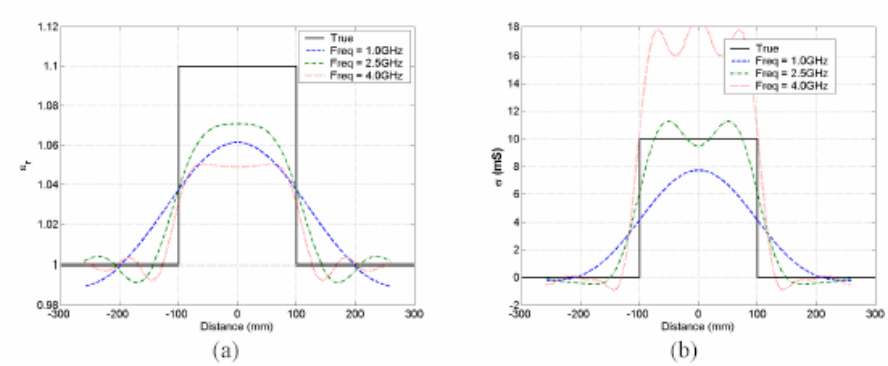

Figure6: The reconstruction of a cylinder with nonzero conductivity. Figure 3(b) should be compared with (a).

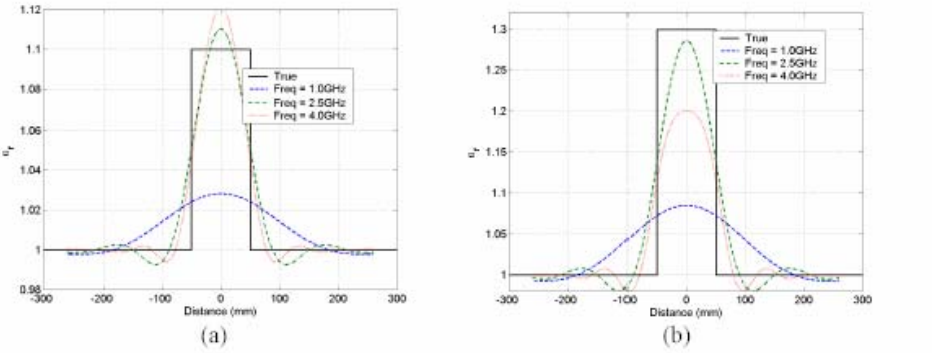

Figure7: The FBP reconstruction of permittivity profile of cylinders with radius=5cm and σ =0.

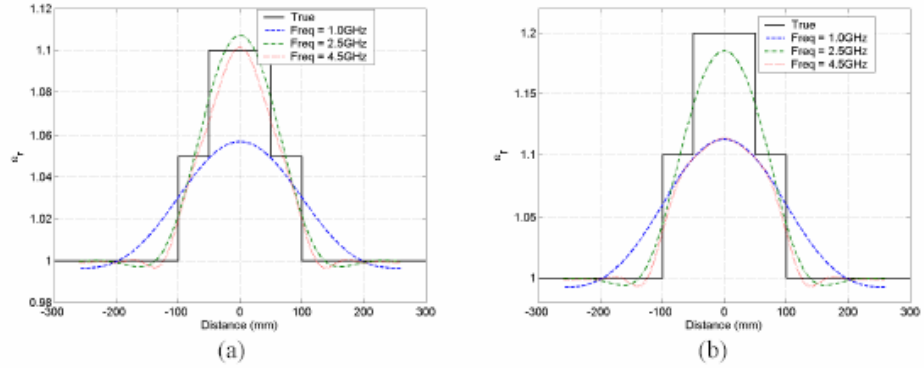

Figure8: Illustration of the Performance of the FBP algorithm in reconstructing cylinders, whose ε_r are changed along their radius. σ =0 for both cases.

The resolution of the FBP imaging is, further, studied in Figures 7 and 8. The FBP cannot produce good results for small objects(Figure 7) and those with more details(Figure 8). One may speculate the reduction in the wavelength would improve the resolution. This, however, increase the Born error, as discussed before.

Finally, we investigate the reconstruction of a 2-D scaled model of a cancerous breast, employing the FBP algorithm. Reported in [18], the relative permittivities of normal and malignant breast tissue Are 10 and 50, respectively. For microwave imaging, the breast is usually inserted into water [3], which forms the background medium. Since the wavelength inside water (ε_r^{water}=80) over microwave frequency is relatively small (λ=3.3 cm at *1GHz*), the simulation of an actual microwave imaging system for breast needs significant computing resources that is not available in our department. Therefore, the simulation is carried out on a scaled model, shown by solid line in Figure 9. All permittivities are divided by 5 so as to preserve the contrast between the elements. In this 2-D model, a 10cm diameter cylinder forms the breast, and the malignant (cancerous) tissue is a cylinder with 8 mm diameter at the center of the breast.

Obviously, it is not expected the FBP make a miracle with such high contrast object. The results is indicated in figure 9, where the failure is evident.

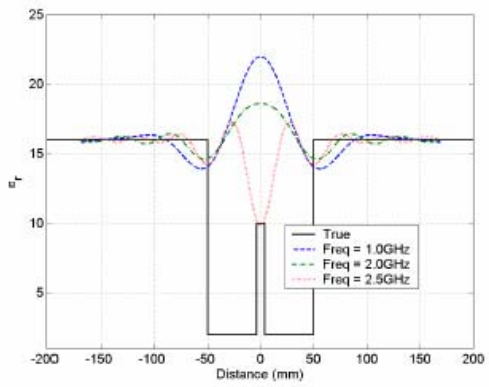

Figure 9: Reconstructing a 2-D scaled model of a cancerous breast, using the FBP algorithm.

The overall conclusion will be presented in the next section.

4 Conclusion

The conventional DT methods suffer from two major drawbacks, lack of sufficient resolution over centimetre wavelength and failure in reconstructing the large objects with considerable contrasts in profile (strong scattering objects). Shortening the wavelength to remedy the resolution problem causes the second problem is more highlighted. The classical DT is, therefore, suitable for weak scattering objects imaged at millimetre wavelengths. This situation arises in several practical applications, such as reconstruction of optical fibers and crystal structures. Further works to solve these problems is going to be ahead in our research.

Acknowledgements

I would like to express my sincere thanks to Dr. M. Nakhkash to have his considerable help with his valuable comments.

References

[1] E.C. Fear, P.M. Meaney, and M.A. Stuchly, "Microwaves for breast cancer detection," *IEEE Potentials*, vol. 22, no. 1, pp. 12-18, Feb.-March 2003.

[2] E.C. Fear, SC. Hagness, P.M. Meaney, M. Okoniewski, and M.A. Stuchly, "Enhancing breast tumor detection with near-field imaging," *IEEE Microwave Magazine*, vol. 3 no. 1, pp. 48-56, March 2002.

[3] P.M. Meaney, M.W. Fanning, D. Li, S.P. Poplack, and K.D. Paulsen, "A clinical prototype for active microwave imaging of the breast," *IEEE Trans. Microwave Theory and Techniques*, vol. 48, no. 11, pp. 1841-53, Nov. 2000.

[4] D. Li, P.M. Meaney, and K.D. Paulsen, "Conformal microwave imaging for breast cancer detection," *IEEE Trans. Microwave Theory and Techniques*, vol. 51, no. 4, pp. 1179-86, April 2003.

[5] S. Caorsi, A. Costa, and M. Pastorino, "Microwave imaging within the second-order Born approximation: stochastic optimiztion by a genetic algorithm," *IEEE Trans. on Antennas & Propagation*, vol. 49, no.1, pp.22-31, Jan. 2001.

[6] S. Caorsi, A. Massa, and M. Pastorino, "Numerical assessment concerning a focused microwave diagnostic method for medical applications," *IEEE Trans. Microwave Theory and Techniques,* vol. 48, no. 11, pp. 1815-30, Nov. 2000.

[7] A.E. Bulyshev, A.E.Souvorov, S.Y. Semenov, R.H. Svenson, A.G. Nazarov, Y.E. Sizov, and G.P. Tatsis, "Three-dimensional microwave tomography. Theory and computer experiments in scalar approximation," *Inverse Problems*, 16, pp. 863-875, 2000.

[8] C. Dourthe, C.Pichot, J.Y. Dauvignac, and J. Cashman, "Microwave imaging of buried objects for ground radar tomography," *Radio Science*, vol. 35, no. 3, pp. 757-771, May-June 2000.

[9] A.J.Devaney, “Geophysical diffraction tomography,” *IEEE Trans. Geosci. Remote Sensing*, vol. GE-22, pp. 3-15, Jan. 1984.

[10] J.R. Jago, and T.A. Whittingham, “Practical system for the application of ultrasound computed tomography to medical imaging,” *IEE Conference Publication*, no. 369, pp. 257-265, 1993.

[11] S.B. Colak, M.B. Mark, G.W. Hooft, J.H. Hoogenraad, E.S. Linden, and F.A. Kuijpers, “Clinical optical tomography and NIR spectroscopy for breast cancer detection,” *IEEE J. Selected Topics Quantum Electronics*, vol. 5, no.4, pp. 1143-58, July/Aug. 1999.

[12] G.A. Tsihrintzis , and A.J. Devaney, “ Higher-order (nonlinear) diffraction tomography: reconstruction algorithms and computer simulation,” *IEEE Trans. Image Processing*, vol. 9, no. 9, pp. 1560-72, Sept. 2000.

[13] Z. Chaoguang, and L. Liu, “Radar-diffraction tomography using the modified quasi-linear,”, *IEEE Tarns. Geosci. Remote Sensing*, vol. 38, no. 1, pp.404-415, Jan. 2000.

[14] R.D. Murch, and T.K.K. Chan, “Improving microwave imaging by enhancing diffraction tomography,” *IEEE Trans. Microwave Theory and Techniques*, vol. 44, no. 3, pp.379-388, Mar. 1996.

[15] R.K. Mueller, M. Kaveh, and G. Wade, “Reconstructive tomography and applications to ultrasonics,” *Proc. IEEE* ,vol. 67, pp. 567-587, Aug. 1979.

[16] S.X. Pan, and A.C. Kak, “A computational study of reconstruction algorithms for diffraction tomography: interpolation versus filtered backpropagation,” *IEEE Trans. Acoustics Speech and Signal Process*., vol. ASSP-31, no.5, pp. 1262-75, Oct. 1983.

[17] A.J. Devaney, “A filtered backpropagation algorithm for diffraction tomography,” *Ultrsonic Imaging*, vol. 4, pp. 336-350, 1982.

[18] X. Li, and S.C. Hagness, “A confocal microwave imaging algorithm for breast cancer detection,” *IEEE Microwave and Wireless Components Letters*, vol. 11, no. 3, pp. 130-132, March 2001.